RESEARCH ARTICLE

National Science Review
12: nwae458, 2025
https://doi.org/10.1093/nsr/nwae458
Advance access publication 11 December 2024

EARTH SCIENCES

Sustainable management of riverine N_2O emission baselines

Shuo Wang[1], Wei Zhi[2], Shengjie Li[3], Tao Lyu[4] and Guodong Ji[1,*]

[1]Key Laboratory of Water and Sediment Sciences, Ministry of Education, Department of Environmental Engineering, Peking University, Beijing 100871, China; [2]The National Key Laboratory of Water Disaster Prevention, Yangtze Institute for Conservation and Development, Key Laboratory of Hydrologic-Cycle and Hydrodynamic-System of Ministry of Water Resources, College of Hydrology and Water Resources, Hohai University, Nanjing 210024, China; [3]Department of Biogeochemistry, Max Planck Institute for Marine Microbiology, Bremen 28359, Germany and [4]School of Water, Energy and Environment, Cranfield University, Cranfield MK43 0AL, UK

*Corresponding author. E-mail: jiguodong@pku.edu.cn

Received 3 July 2024; **Revised** 27 November 2024; **Accepted** 10 December 2024

ABSTRACT

The riverine N_2O fluxes are assumed to linearly increase with nitrate loading. However, this linear relationship with a uniform EF_{5r} is poorly constrained, which impedes the N_2O estimation and mitigation. Our meta-analysis discovered a universal N_2O emission baseline ($EF_{5r} = k/[NO_3^-]$, $k = 0.02$) for natural rivers. Anthropogenic impacts caused an overall increase in baselines and the emergence of hotspots, which constitute two typical patterns of anthropogenic sources. The k values of agricultural and urban rivers increased to 0.09 and 0.05, respectively, with 11% and 14% of points becoming N_2O hotspots. Priority control of organic and NH_4^+ pollution could eliminate hotspots and reduce emissions by 51.6% and 63.7%, respectively. Further restoration of baseline emissions on nitrate removal is a long-term challenge considering population growth and declining unit benefits ($\Delta N\text{-}N_2O/N\text{-}NO_3^-$). The discovery of EF lines emphasized the importance of targeting hotspots and managing baseline emissions sustainably to balance social and environmental benefits.

Keywords: nitrous oxide, emission factor, hotspots, sustainable, greenhouse gases

INTRODUCTION

In the Anthropocene epoch, agriculture and rapid urbanization completely alter the natural nutrient conservation mechanism under the impact of clearing natural vegetation and introducing excessive nutrients. Increasing N availability in global rivers leads to unintended environmental consequences, including increased nitrous oxide (N_2O) emissions [1,2]. Global rivers thereby become a significant anthropogenic source for N_2O emissions. Estimates indicate that global riverine N_2O emissions have experienced a 4-fold increase since the 1900s [2]; this rate of increase is three times faster than terrestrial ones [2], contributing 10%–30% to the overall anthropogenic N_2O budget [3,4].

In the estimation and management of indirect N_2O emissions (The Intergovernmental Panel on Climate Change (IPCC)), riverine N_2O fluxes are commonly assumed to linearly increase with nitrate loading on the basis of the emission factor EF_{5r} ($[N_2O]/[NO_3^-]$) [5,6]. EF_{5r} has been constantly refined by the IPCC from 0.75% (1998) to 0.25% (2006) and to 0.26% (2019). However, recent studies have continued to argue that the current default EF_{5r} may either overestimate or underestimate the riverine N_2O emissions [6–8]. Although riverine N_2O emissions tend to increase with N inputs, this linear relationship with a uniform EF_{5r} (0.26%) is often weak or non-existent [9,10]. Moreover, the observed EF_{5r} is poorly constrained due to the high heterogeneity of global rivers, ranging from 0.005% to 7% [4,11]. As a result, uncertainties will inevitably widen when extrapolating the simplistic factor for the global estimation. Additionally, our understanding of riverine N_2O emissions remains fragmented with a bias towards N-rich rivers, yet no clear large-scale pattern has been identified for global rivers [9]. This simplistic and fragmented understanding thereby hinders our ability to comprehend the underlying mechanism of riverine N_2O emissions and quantify human impacts. This, in turn, impedes the development of effective mitigation strategies.

Agricultural production, animal husbandry, industrial and domestic sewage are the major sources of general nitrogen and organic pollution in rivers. The continuous urbanization, increasing food demand and widespread deoxygenation in warming rivers will further increase N_2O emissions [12–15].

The current emission factor EF_{5r} ($[N_2O]/[NO_3^-]$) emphasizes the importance of reducing nitrate in N_2O emission mitigation. However, the broad range of EF_{5r} underscores the complexity of microbial processes and environmental factors regulating riverine N_2O emissions. Riverine production of N_2O greatly depends on microbial activity, particularly nitrification, nitrifier denitrification (NDN) and denitrification processes [16]. Incomplete denitrification is commonly assumed to be the dominant pathway regulating N_2O production and consumption in rivers [6,17]. However, denitrification activity in aquatic ecosystems is generally limited by the supply of electron donors (organic matter) rather than NO_3^- [18]. Whether the introduction of excess nitrate can linearly increase N_2O production, as well as the role of organic carbon, requires further investigation. Additionally, recent research has emphasized nitrification as a non-negligible source of N_2O emissions in rivers and lakes [19,20]. NH_4^+-derived pathways were even proven to be the dominant N_2O sources in low-order agricultural streams around the world [21]. These findings collectively challenge the prevailing management priorities regarding nitrate. Therefore, we hypothesize that organic pollutants and ammonia may also play an important role in the management of riverine N_2O emissions, which have been underestimated in previous models.

It is worth noting that the IPCC method provides policymakers with convenient and easy-to-use parameters for regional and global N_2O emission estimations [22]. Consequently, it has been widely applied with a large-scale dataset [23–46]. Previous studies have proposed a variety of non-linear models, including efficiency loss models and exponential models, for refinement of emission factor estimates [7]. The extensive range of EF_{5r} presents an opportunity for the extraction of valuable insights through data mining. To do so, we conducted a comprehensive global meta-analysis including 3047 *in situ* measurements across different river types (natural, agricultural and urban rivers) to explore the intrinsic nature of EF_{5r}. Seasonal measurements of N_2O fluxes and isotopic signatures were also performed in rivers impacted by anthropogenic activities (agriculture and urbanization) to determine the prevailing microbial processes and predominant environmental drivers. Finally, in this study, a global distribution map of N_2O hotspots with effective management strategies was generated. This study can enhance our understanding of how human activities impact global riverine N_2O emissions and address the questions of how much of these emissions can be mitigated and how to do so most effectively.

RESULTS

Universal EF lines for global rivers

The determination of N_2O emissions for highly heterogeneous rivers has long remained a contentious issue. The IPCC adopted a value of 0.26% ($n = 91$) as a representation of the global riverine emission factor [47]. Through the analysis of a comprehensive dataset comprising 3047 observations, it was revealed that EF_{5r} varies by five orders of magnitude (Fig. 1a), with an average value of 0.50% (Fig. 1b), which is greater than that adopted by the IPCC. Importantly, our results indicated that the EF_{5r} value adopted by the IPCC cannot be universally applied across all rivers, because EF_{5r} exhibits significant variations across different river types. The EF_{5r} of natural rivers without human influence (0.79%) was notably greater than that of agricultural rivers (0.06%) and urban rivers (0.18%), leading to both overestimation and underestimation of EF_{5r} in specific river categories. These findings emphasize the importance of considering the distinct characteristics of different river types when estimating N_2O emissions.

Furthermore, it was revealed that EF_{5r} decreased with increasing NO_3^- concentration (Fig. 1c), precisely conforming to the inversely proportional function $EF_{5r} = k/[NO_3^-]$ ($R^2 = 0.90$) for natural rivers, hereafter referred to as the EF baseline. A k value of 0.02 represents situations without human disturbance. At the baseline, N_2O concentrations are insensitive to further increases in nitrate levels, but are determined by the k value ($EF_{5r} = k/[NO_3^-] = [N_2O]/[NO_3^-]$, that is $[N_2O] = k$). Iterative analyses were further conducted on individual watersheds (Fig. S1a–j), and the k values were positively correlated with the average nitrate concentration in rivers (Fig. S1k, $R^2 = 0.78$, $P < 0.001$). Therefore, the k value could serve as a reference for the overall nutrient level and basic N_2O emissions in rivers. In other words, the average nitrate concentration determines the basic N_2O emissions in rivers.

Regarding agricultural and urban rivers, anthropogenic impacts caused an overall increase in their baselines and the emergence of hotspots (Fig. 1d and e, Figs S2–S3). To obtain baselines, outliers were excluded according to the 3σ rule in each fitting iteration (Tables S1–S2). The k values of agricultural and urban rivers increased to 0.09 and 0.05, respectively, which is consistent with the increase in nutrient levels. The plot of measured EF_{5r} versus predicted EF_{5r} values illustrates the reliability of EF lines (Fig. 2a–c). Notably, most outliers that deviated from the baseline became N_2O hotspots in agricultural (11%) and urban rivers (14%). Several outliers occurred below the fitting line, especially in agricultural rivers,

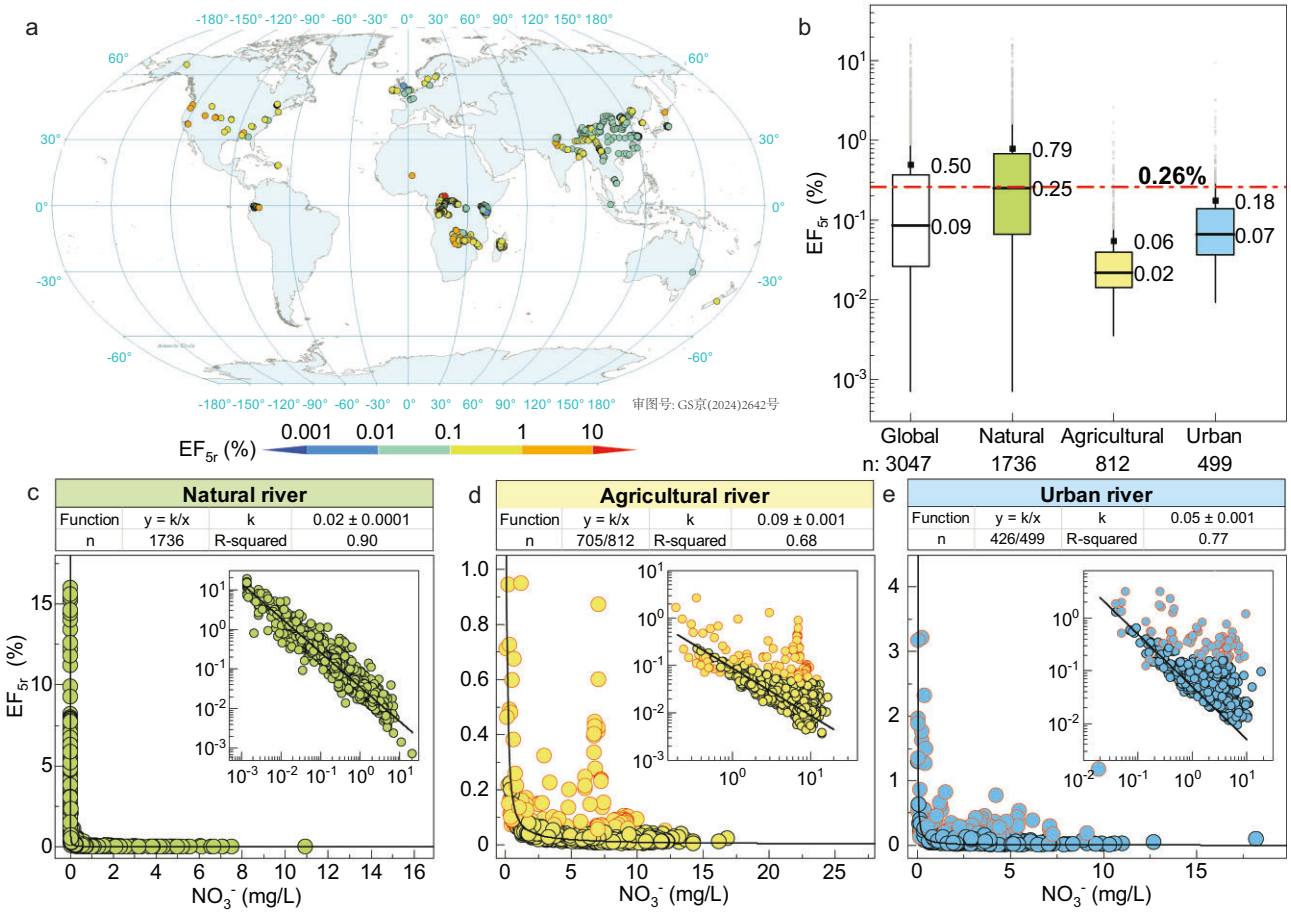

Figure 1. Location and characteristics of EF_{5r} used in the meta-analysis. (a) Geographical distribution of EF_{5r} from the global riverine sample sites. (b) EF_{5r} of global rivers and variations across different river types (natural, agricultural and urban rivers). The boxes are bounded by the 25th and 75th percentiles. The whiskers represent 1.5 × the interquartile range, and the solid line denotes the median. The black dots denote arithmetic means, and the gray dots denote outliers. (c-e) EF lines with k values indicating nutrient levels and basic N_2O emissions in the different rivers. The model function y = k/x was employed for fitting. In each iteration, a residual analysis was performed to exclude any points deviating from the baseline (3σ rule) until there were no outliers in the fitted curve. n indicates the points without outliers/total sampling points.

which are probably caused by natural factors (e.g. waterfalls or rainstorms) or human activities (e.g. irrigation). When anthropogenic impacts exist, EF_{5r} significantly deviates from the baselines and cannot be accurately predicted with nitrate as the only variable (Fig. 2d and e). Overall, the baseline emissions and hotspots constitute two typical patterns of anthropogenic sources in global rivers. To reveal the underlying mechanism of the two typical N_2O emission patterns, regional investigations based on isotopes and meta-analyses of the physicochemical parameters of global rivers were performed.

N_2O baseline emissions

During the initial phase of the baselines, even minor amounts of NO_3^- were accompanied by a certain $N_2O_{equilibrium}$ level, resulting in extremely high emission factors near the zero point, especially for natural rivers (Fig. 1c). Subsequently, EF_{5r} decreased with increasing NO_3^- concentration. Therefore, an increase in nitrate does not necessarily lead to increased N_2O emissions. Similar phenomena have been observed in rivers and estuaries and have been attributed to biological saturation [7,13]. To reveal the underlying mechanism, the microbial sources of N_2O production in anthropogenically impacted rivers were quantified by isotopic approaches (Figs S4–S6), which can provide an insight into N_2O production and reduction mechanisms [48–50]. In Haihe River basin, the EF baseline was established with the function y = 0.045/x (Fig. S6a, R^2 = 0.91). Isotopic signatures of N_2O, $\delta^{15}N^{Bulk}$, $\delta^{18}O$ and $\delta^{15}N^{SP}$ were combined to separate N_2O microbial sources in 3D isotope space (Fig. S6b). For the sampling points around the baseline,

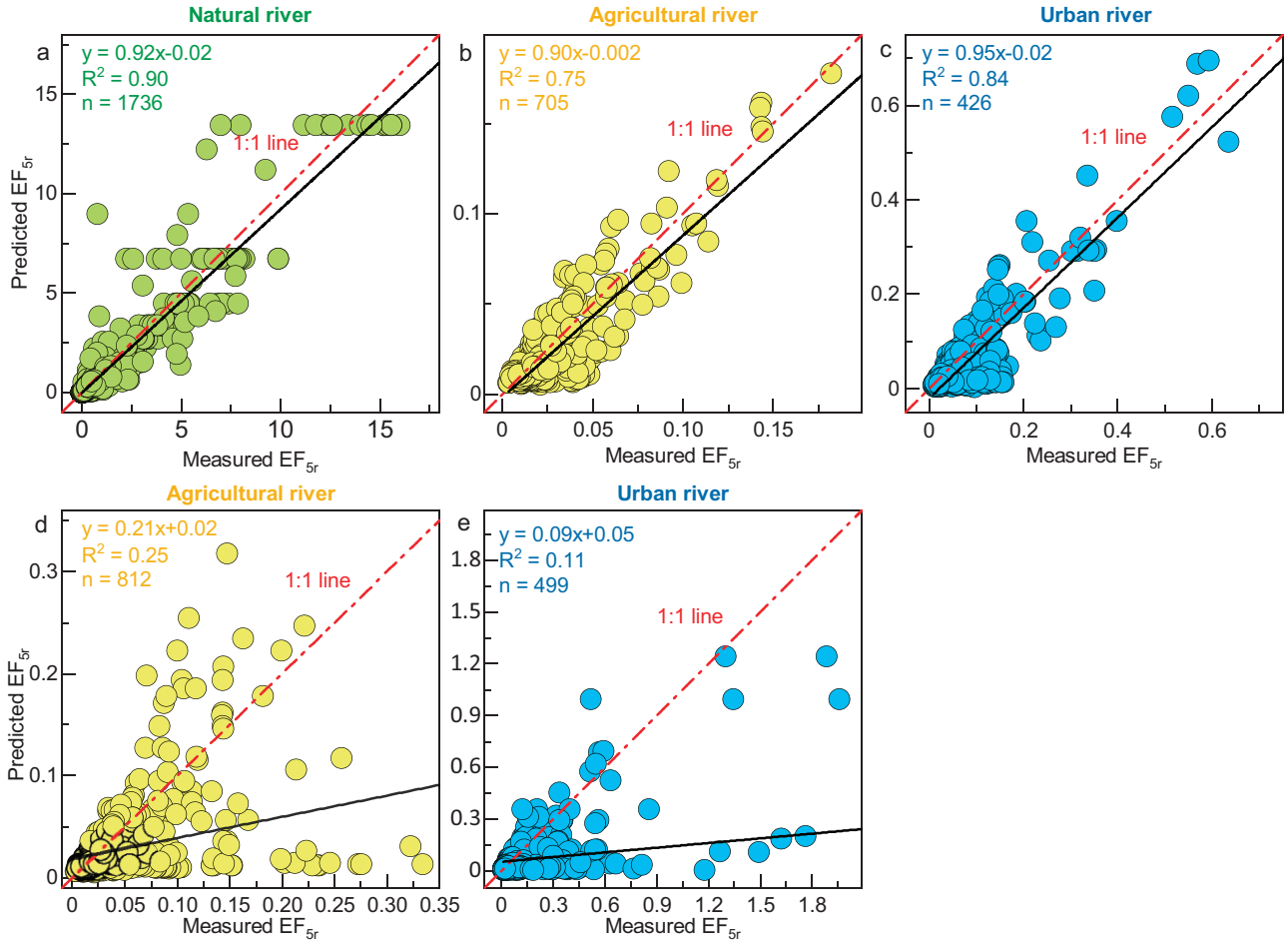

Figure 2. Measured versus predicted EF_{5r} values. (a-c) The riverine sampling points without outliers. (d, e) All the sampling points. The red dotted line denotes the 1:1 line. The black line denotes the linear regression fit, and R^2 is the coefficient of determination.

nitrification significantly contributed to N_2O emissions (51.7%), thereby a decrease in the NH_4^+/NO_3^- ratio led to a decrease in EF_{5r} ($[N_2O]/[NO_3^-]$) (Fig. S6c and d). Similarly, denitrification accounted for an average contribution of 39.2% to N_2O emissions for baseline points (Fig. S6c). As NO_3^- reduction typically occurs only when there are sufficient electron donors [18,51], excessive nitrate is rendered inert nitrogen. Therefore, the decreasing dissolved organic carbon (DOC)/NO_3^- ratio with nitrate limits the production of N_2O, further resulting in a decrease in EF_{5r} (Fig. S6e). From the regional to global scales, the NH_4^+/NO_3^- and DOC/NO_3^- ratios jointly determine the EF_{5r} according to significant linear relationships, and the inversely proportional decreases in the NH_4^+/NO_3^- and DOC/NO_3^- ratios with increasing NO_3^- finally determine the distribution of the EF baselines (Fig. S7).

The baseline N_2O emissions were characterized by specific k values in the different types of rivers (Fig. 3 and Fig. S8). In natural rivers, the surrounding terrestrial vegetation and internal carbon/nitrogen cycle are the major sources of nitrogen (NH_4^+ and NO_3^-) and organic matter [52]. They are generally subject to the overall nutrient level in the system, with the total nitrogen (TN; comprising mainly nitrate) as one of the main limiting factors. Therefore, natural rivers effectively sequester and recycle N at relatively low nutrient levels (k = 0.02) due to the extremely limited N availability (median NO_3^- = 0.3 mg/L). The difference in the N_2O partial pressure ($\Delta N_2O = N_2O_{water} - N_2O_{equilibrium}$) was used to indicate the N_2O emission capacity of global rivers. The natural source of riverine N_2O emissions was negligible, with a median ΔN_2O concentration of 0.02 nM. Geographically, most high-order natural rivers, such as the Napo River, Yellow River, Yangtze River and Ganges River, generally exhibit low levels of baseline N_2O emissions, even functioning as sinks of atmospheric N_2O (Fig. 4e). By contrast, agriculture and urbanization introduce excessive

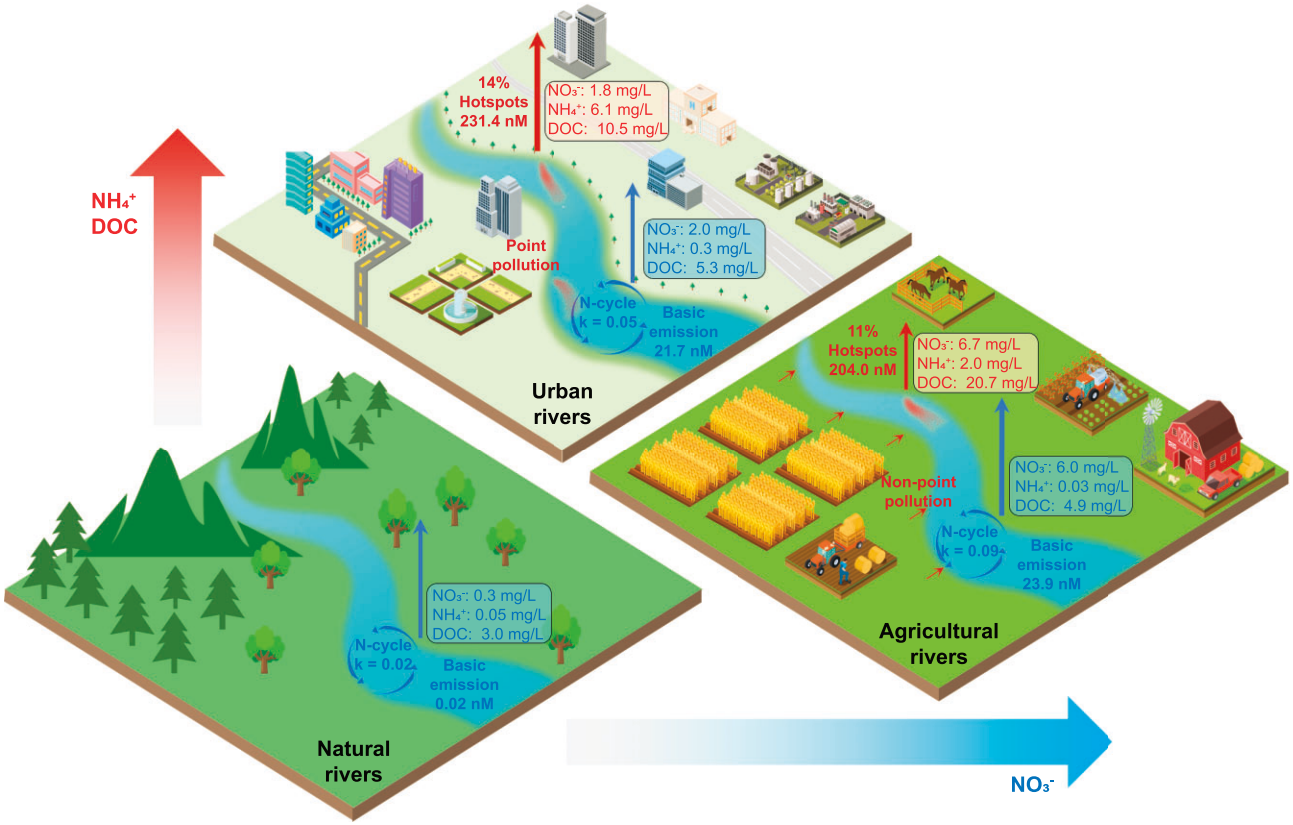

Figure 3. Natural and anthropogenic N_2O emissions. Anthropogenic sources constitute the primary component of N_2O emissions in global rivers and are mainly manifested as two patterns: baseline emissions and localized hotspots. The k values of the EF lines for natural, agricultural and urban rivers were determined at 0.02, 0.09 and 0.05, respectively, indicating increasing nutrient levels and basic N_2O emissions in the different types of rivers. The corresponding median ΔN_2O concentrations were 0.02, 23.9 and 21.7 nM, respectively. The median NH_4^+, NO_3^- and DOC concentrations for the basic emissions (blue) and localized hotspots (red) are shown for the different rivers. Additionally, the median ΔN_2O concentration at localized hotspots reached 204.0 nM (11%) and 231.4 nM (14%) in agricultural and urban rivers, respectively.

nutrients into rivers. The median NO_3^- concentration for the agricultural baseline points was 6.0 mg/L, which is significantly greater than that of the other rivers (Fig. 3). Although it is difficult for inert nitrates to be directly reduced in aerobic rivers with insufficient electron donors, elevated nutrient levels could determine the primary productivity of phytoplankton and surrounding terrestrial vegetation, thereby promoting basic N_2O emissions with an increased k value of 0.09. Similarly, the moderate TN level (median NO_3^- = 2.0 mg/L) in urban rivers caused an increase in the k value to 0.05. The corresponding median ΔN_2O concentrations in agricultural and urban rivers were 23.9 and 21.7 nM, respectively, which are significantly greater than those in natural rivers. It is worth noting that the baseline N_2O emissions in agricultural rivers are significantly higher than those in urban rivers, largely due to the substantial leaching of fertilizer from agricultural non-point sources.

Localized hotspots

The hotspots are generally derived from sudden increases in organic and NH_4^+ loads. In the case of the identified hotspots (Fig. S6a, Spring-CB1 and Autumn-CB5), organic pollution activates nitrate, leading to a significant increase in denitrification activity (Fig. S6c). Because NH_4^+ pollution often occurs simultaneously with organic pollution (Fig. S9), the introduction of NH_4^+ also significantly contributes to N_2O production through nitrification and nitrifier denitrification. Therefore, sampling points where the NH_4^+/NO_3^- and DOC/NO_3^- ratios deviated from the fitting lines potentially became hotspots of N_2O emissions (Fig. S6d and e). Globally, the NH_4^+ and DOC concentrations in hotspots were significantly greater than those at the baseline points, especially for the NH_4^+/NO_3^- and DOC/NO_3^- ratios (Fig. S8b–e).

Although only a few of the sampling points became hotspots in agricultural (11%) and urban

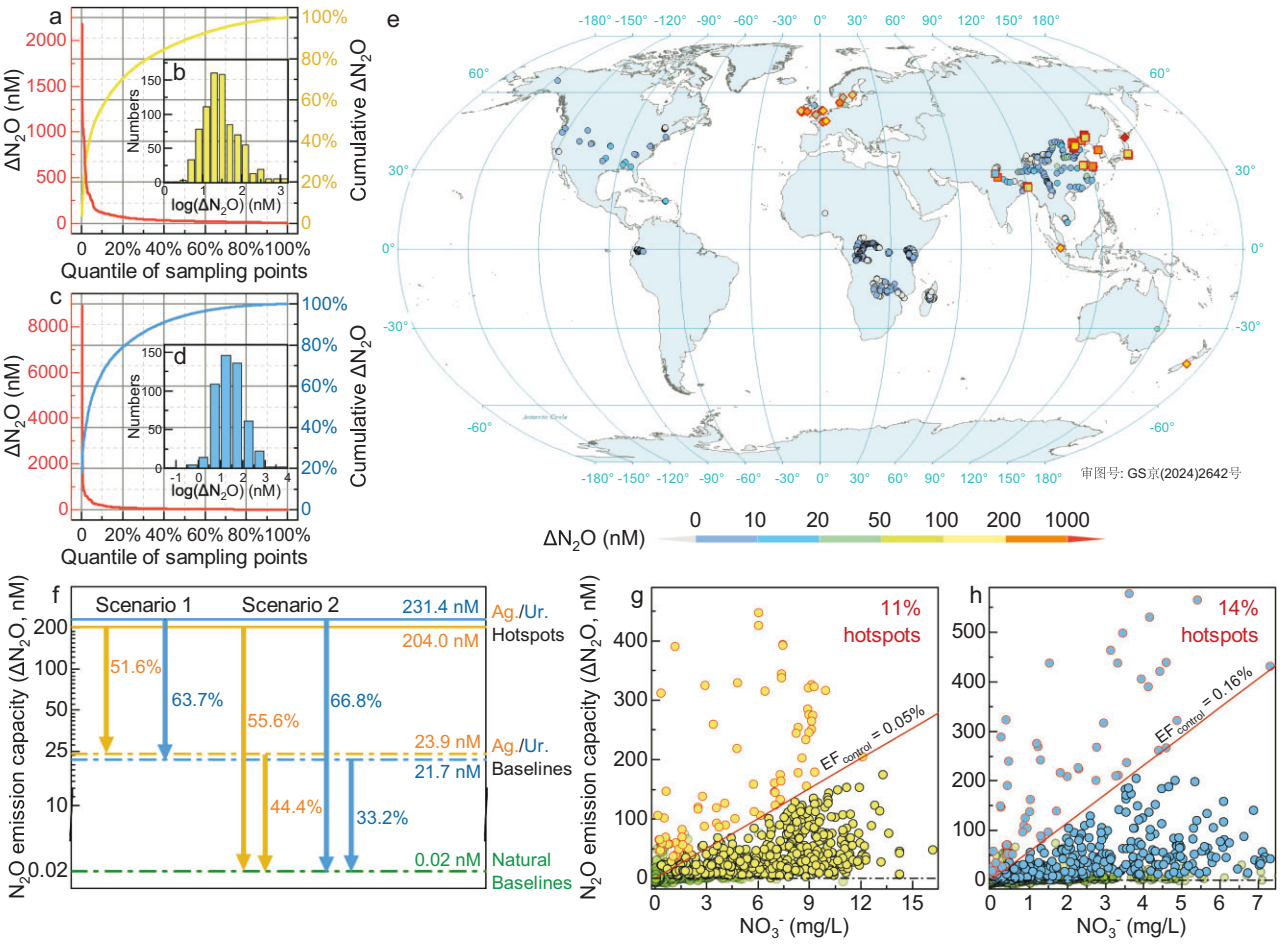

Figure 4. Effective management strategies. (a, c) $\Delta N\text{-}N_2O$ concentration (red lines), and cumulative $\Delta N\text{-}N_2O$ (yellow/blue lines) for different quantiles of sampling points; (b, d) Log-normal distribution of $\Delta N\text{-}N_2O$ in agricultural and urban rivers; (e) Geographical distribution of N_2O emissions (ΔN_2O) in global rivers. The diamonds and squares with red borders denote the hotspots in agricultural and urban rivers, respectively. (f) Scenarios for the management of riverine N_2O emissions. (g, h) Nitrate-based ΔN_2O reduction model. The green, yellow and blue points denote the sampling points in natural, agricultural and urban rivers, respectively. The points with red borders indicate N_2O hotspots, and the slope ($\Delta N\text{-}N_2O/N\text{-}NO_3^-$) represents the unit benefit of N_2O emission reduction caused by treating a unit of nitrate.

(14%) rivers, the median ΔN_2O concentrations reached 204.0 and 231.4 nM, respectively (Fig. 3 and Fig. S8), almost 10 times the basic emission levels. The hotspot emissions in urban rivers are more severe than those in agricultural rivers due to the greater impact of point source pollution in urban areas. Statistically, a log-normal probability distribution for the $\Delta N\text{-}N_2O$ concentration was observed in agricultural and urban rivers (Fig. 4a–d), indicating the disproportionate contributions of hotspots at the tail of these frequency distributions. Therefore, targeting pollution control towards the high ends of these distributions would probably result in greater environmental gains per unit of management effort. In contrast to natural rivers, low-order streams contributed disproportionate amounts to N_2O emissions due to the massive amounts of terrestrially derived carbon/nitrogen inputs (Fig. 4e). Agricultural N_2O hotspots were mainly distributed in Asia and Europe, which exhibit intensively cultivated croplands and dense populations. Moreover, urban hotspots were significant in megacities, such as Beijing, Shanghai, Tokyo and New Delhi, while no significant urban hotspots were observed in developed countries, such as the USA, Canada and in Europe. Because the point source pollution in urban areas is comparatively more manageable than non-point source pollution in agricultural rivers, developed countries have basically eliminated hotspot emissions in urban rivers, but still experience hotspot emissions caused by agricultural non-point source pollution. Additionally, due to the lack of monitoring sites, potential hotspots in certain developing countries are not shown on the map.

DISCUSSION

Anthropogenic perturbations in nitrogen flow have exceeded the proposed planetary boundary [53], leading to concomitant threats to agricultural productivity, food security, global climate and economic prosperity [54]. We are trying to explain how N_2O is emitted from global rivers and how to reduce it using the simplest mathematical curve. The discovery of EF lines helps us better understand how human activities affect global riverine N_2O emissions and aids in the development of effective management strategies.

Riverine N_2O emission patterns

The discovery of EF lines reveals the two typical patterns of anthropogenic N_2O sources in global rivers: an overall increase in baselines and the emergence of hotspots. At the baseline, accurate predictions of EF_{5r} are feasible for rivers with the function $EF_{5r} = k/[NO_3^-]$ (Fig. 2a–c). The riverine N_2O concentration was insensitive to further increases in nitrate levels but was determined by the k value. The k value is generally determined by the overall nutrient level in rivers, mainly by the nitrate concentration. Therefore, nitrate removal is the key point for mitigating baseline N_2O emissions. However, the existence of hotspots caused the measured EF_{5r} to significantly deviate from the baseline trend, and EF_{5r} cannot be accurately predicted with nitrate as the only variable (Fig. 2d and e). As we hypothesized, organic pollution and NH_4^+ play an important role in the riverine N_2O emissions. Organic matter rapidly activates nitrate, accompanied by simultaneous NH_4^+ input (Fig. S9), leading to a significant increase in N_2O emissions. In contrast to the basic N_2O emissions with time lags, localized hotspots can exhibit excessive N_2O emissions within a short time, where anthropogenic pollution might exceed the environmental carrying capacity, accompanied by irreversible changes and serious degradation in ecosystems (e.g. algal blooms and black-odor water). Therefore, restoring hotspots might return their original ecological functions and provide additional ecological benefits.

Two scenarios for mitigating riverine N_2O emissions

Two scenarios (Fig. 4f) were established to answer the following questions: How much can riverine N_2O emissions be mitigated? How can they be mitigated more effectively?

Scenario 1: Restore the agricultural/urban hotspots (204.0/231.4 nM) to their baselines (23.9/21.7 nM) by controlling organic and NH_4^+ pollution. Despite similar nitrate concentrations between hotspots and baseline points, the excessive presence of DOC and NH_4^+ results in significant N_2O emissions (Fig. 3 and Fig. S8). Therefore, controlling organic and NH_4^+ pollution can restore agricultural/urban hotspots to their baseline levels without further nitrate removal. As a result, restoring hotspots in agricultural (11%) and urban (14%) rivers could reduce N_2O emissions by 51.6% and 63.7%, respectively. Even in agricultural rivers dominated by non-point source pollution, critical source areas often contribute most to the pollution load in the entire watershed.

Scenario 2: Restore the agricultural/urban hotspots and their baselines to the natural baselines (0.02 nM). In addition to organic and NH_4^+ pollution control, further nitrate removal is needed to completely eliminate N_2O emissions in rivers (Fig. 3 and Fig. S8). In this case, restoring hotspots to the natural baselines in agricultural and urban rivers could reduce N_2O emissions by 55.6% and 66.8%, respectively. This is only slightly higher than in Scenario 1 (51.6% and 63.7%), but was achieved at a greater cost for additional nitrate removal. Additionally, the further restoration of remaining baselines needs to manage more than 80% sampling points, but could only reduce N_2O emissions by 44.4% and 33.2% in agricultural and urban rivers, respectively.

From the perspective of nitrate removal (Fig. 4g and h), the slope represents the benefit of N_2O emission reduction achieved by treating a unit of nitrate ($\Delta N\text{-}N_2O/N\text{-}NO_3^-$). Obviously, the hotspots identified by the EF lines exclusively occurred in the upper left, the elimination of which provided the greatest unit benefit of 0.25% and 0.69% in agricultural and urban rivers, respectively (Table S4). Instead of mechanical restoration from the highest $\Delta N\text{-}N_2O$ concentration, our model considered a more efficient mitigation strategy on the order of unit benefits (slope, $\Delta N\text{-}N_2O/N\text{-}NO_3^-$). Moreover, we found that the thresholds for N_2O hotspot control ($EF_{Control}$, $\Delta N\text{-}N_2O/N\text{-}NO_3^-$) in agricultural and urban rivers were 0.05% and 0.16%, respectively. These values can easily be applied as a reference for the identification and management of N_2O hotspots. However, further restoration of the baseline points with decreasing slopes resulted in a steep decrease in the unit benefits (Table S4). Thereby, restoring the baseline points could only reduce N_2O emissions by 44.4% and 33.2% in agricultural and urban rivers, respectively (Fig. 4f). In contrast to hotspots with severe organic pollution, nitrate removal at the baseline points also requires additional electron donors. Therefore, mitigation strategies for

both agricultural and urban rivers should first focus on eliminating organic and NH_4^+ pollution at hotspots, while nitrate removal provided lower unit benefits for N_2O mitigation but came at a greater cost.

Sustainable management strategies

The sustainable management of N_2O should integrate environmental, social and economic considerations into the decision-making process. According to the definition of EF_{5r} (IPCC), N_2O emissions were assumed to linearly increase with nitrogen loading. In this case, nitrate removal is crucial for controlling N_2O emissions. However, our results suggested that targeting hotspot elimination would probably result in greater environmental value. It is thereby recommended to first restore agricultural/urban hotspots to their baselines and then restore their baselines to the natural baselines. In other words, in regions with significant N_2O hotspots, controlling organic and NH_4^+ pollution should be prioritized. Compared with nitrate, the treatment of organic and NH_4^+ pollution is easier and less costly. The priority control of organic and NH_4^+ pollution could rapidly eliminate N_2O hotspots and halve its total emissions. This finding is of great significance to practical engineering and aids in the development of more effective management strategies.

The point source pollution in urban areas is comparatively more manageable. Based on data from the United Nations Sustainable Development Goals (SDG 6, clean water and sanitation) [55], the sewage collection rate is more than 90% in developed countries, thereby no significant urban hotspots were observed (Fig. 4e). By contrast, the collection rate is less than 60% in most developing countries, especially India (21%), which hosts a large population, thereby leading to the situation of being besieged by N_2O hotspots (Fig. 4e). In the future, well-managed urbanization, including land intensification, the improvement of sewage collection and an expansion of wastewater treatment capabilities, will be favorable for rapidly eliminating hotspots in developing countries. However, managing non-point source pollution in rural areas is challenging. It has been reported that ∼60% of the fertilizer applied in soils leaches into stream systems [21]. Therefore, certain developed countries, such as Japan, New Zealand and those in Europe, still experience hotspot emissions caused by agricultural non-point source pollution. This phenomenon is more serious in developing countries. For example, China has long been the largest NH_4^+ fertilizer consumer in the world [21]; large numbers of agricultural hotspots have been observed in the Beijing-Tianjin region and the Yangtze River Delta. Currently, most measures are restricted and rarely implemented due to socioeconomic barriers, such as small farm size [56]. The continued urbanization leads to rural depopulation, both through rural-to-urban migration and natural aging, benefiting the ongoing increase of large-scale farming practices. It has been estimated that the proportion of large-scale cropland farms could increase from 9% in 2017 to 90% by 2050 in China, thus improving cropland nitrogen use efficiency from 43% to 54% [57]. Overall, agricultural centralization and the identification of critical source areas are important for managing N_2O hotspots in agricultural watersheds [58].

The priority control of organic and NH_4^+ pollution could rapidly eliminate global riverine N_2O hotspots and reduce emissions by one-half. After eliminating hotspots, the management of baseline emissions is notably constrained by social and economic development. Considering population growth and the massive demand for fertilizer, nitrate will inevitably be leached from intensive arable systems. For instance, the median NO_3^- concentration at the agricultural baseline points was 6.0 mg/L, 20 times the natural level of 0.3 mg/L. Mitigating baseline emissions requires long-term investment but yields lower unit benefits. Fortunately, our EF lines demonstrate that the ecosystem can balance and withstand moderate anthropogenic pressure with increased k values. Moreover, too little N could lead to lower crop productivity and poor human nutrition. As a result, nitrate concentrations can remain at appropriate high levels within the environmental carrying capacity, where a greater N cycle and primary production favor rapid N removal and self-restoration.

MATERIALS AND METHODS

Data collection and sampling sites

A literature search was conducted using bibliographic databases (Web of Science, Google Scholar, etc.) for papers containing data on N_2O concentrations and indirect N_2O emission factors (EF_{5r}) for global rivers (from 2000 to 2023) [23–46]. In total, our efforts identified ∼3000 river points with N_2O, NO_3^-, NH_4^+ and DOC concentrations. In addition to literature data, N_2O-related parameters from large river networks in China were also measured (https://thesis.lib.pku.edu.cn/). A list of the cited and measured data is provided in the Supplementary Data. To further reveal anthropogenic impacts on N_2O emission, a seasonal measurement of N_2O fluxes and isotope values in the Haihe River basin was conducted to reveal the underlying process and the main environmental regulators

controlling EF_{5r}. *In situ* measurements were conducted in two major rivers within the Haihe River basin, namely, the YongDing River and ChaoBai River, which are significantly impacted by urbanization and agriculture (Fig. S4). This region exhibits a continental monsoon climate characterized by an annual precipitation of ∼600 mm and an average annual temperature of 10−12°C [3]. Triplicate water samples were collected from rivers during ice-free periods, and seasonal sampling was performed during the spring (April), summer (July) and autumn (October) seasons of 2022. In total, 108 observations were obtained during the sampling campaigns. No abnormal hydrological variations or extreme weather events were recorded during the sampling periods.

Establishment of the EF-line model

According to the river type, we divided the collected data into natural, agricultural and urban river data. Only field observations with original data were used for further fitting. The non-linear relationship between the EF_{5r} value and NO_3^- concentration was fitted using the non-linear curve fit option in Origin 2020 via the Levenberg–Marquardt algorithm. The model function $y = k/x$ was employed for fitting. A residual analysis was performed to exclude any points deviating from the baseline. In each iteration, sampling points with residual errors greater than three times the standard deviation were identified as outliers (3σ rule). Outliers were excluded, and the remaining points were again fitted at each time point until there were no outliers in the fitted curve (Tables S1–S2). EF lines of natural, agricultural and urban rivers were finally obtained via iterations (Figs S1–S3), with the outliers highlighted in red in the Supplementary Data. In addition, EF lines of individual rivers were obtained in the same way.

Physicochemical parameters and dissolved N_2O

A precalibrated portable multiparameter device (DZB-718, Leici, China) was used to record the water temperature, pH, dissolved oxygen (DO), oxidation-reduction potential and electrical conductivity (EC) simultaneously. Subsequently, all water samples were stored at 4°C during transport to the laboratory. Subsequently, the water samples were filtered through 0.22-μm polyethersulfone syringe filters. An ultraviolet spectrophotometer (UV5100, Shanghai, China) was employed for the determination of NH_4^+ (Nessler's reagent spectrophotometry method), NO_2^- (diazamine coincidence spectrophotometry) and NO_3^- (ultraviolet spectrophotometric method). The DOC concentration was determined using a total organic carbon (TOC) analyzer (TOC-L, Shimadzu, Japan). The dissolved concentrations of N_2O in the freshwater samples were measured by an Agilent 7890B gas chromatograph (Agilent 7890B, μECD) using the headspace equilibrium method [59]. The temperatures of the oven, chromatographic column and the detector were kept constant at 70, 280 and 330°C, respectively. The dissolved N_2O concentration in the water samples (N_2O_{water}) was calculated based on the partial pressure of N_2O in the headspace and Henry's law constant for N_2O (Eq. 1) [60]:

$$N_2O_{water} = C_g \times \left(\frac{V_g}{V_l} + K_h RT\right), \quad (1)$$

where C_g is the measured N_2O concentration in the headspace (nmol/L); N_2O_{water} is the calculated dissolved N_2O concentration (nmol/L); V_g and V_l are the gas and liquid volumes, respectively (mL); K_h is Henry's law constant, which is calculated as $K_h = K_{h0} \times \exp\left(2700 \times \left(\frac{1}{T} - \frac{1}{298.15}\right)\right)$ (mol m^{-3} pa^{-1}); K_{h0} is Henry's law constant at the standard temperature (T = 298.15), which is equal to 2.4×10^{-4} (mol m^{-3} pa^{-1}); R is the ideal gas constant, which is equal to 8.314472 m^3 Pa/(K mol); and T is the water temperature (K).

Measurements and processing of N_2O isotopic signatures

In recent years, stable isotopes have been widely used to reveal the underlying mechanism of riverine N_2O emissions [19,20,61,62], which offer quantitative information on N transformation and N_2O sources. To obtain the $\delta^{15}N^{Bulk}$, $\delta^{18}O$ and $\delta^{15}N^{SP}$ values of N_2O, the gas samples were introduced into an isotope ratio-monitoring mass spectrometer (GC-IRMS; Delta V Plus, Thermo Fisher Scientific, Bremen, Germany). Calibration was conducted by measuring the N_2O standards (330 ppb; $\delta^{15}N^{\alpha}$, −0.4‰; $\delta^{15}N^{\beta}$, −0.15‰; $\delta^{15}N^{Bulk}$, −0.28‰; $\delta^{18}O$, 41.95‰; Air Liquide America, Specialty Gases LLC). The isotope ratios of N_2O in delta (δ) notation were used for analysis and are presented in units of per mil (‰), as expressed in Eqs. 2–5:

$$\delta^{15}N^{Bulk} = \left[\left({}^{15}N/{}^{14}N\right)_{sample}/\left({}^{15}N/{}^{14}N\right)_{reference} - 1\right] \times 1000 \quad (2)$$

$$\delta^{15}N^{\beta} = 2 \times \delta^{15}N^{Bulk} - \delta^{15}N^{\alpha} \quad (3)$$

$$\delta^{15}N^{SP} = \delta^{15}N^{\alpha} - \delta^{15}N^{\beta} \quad (4)$$

$$\delta^{18}O = \left[\left({}^{18}O/{}^{16}O\right)_{sample}/\left({}^{18}O/{}^{16}O\right)_{reference} - 1\right] \times 1000. \quad (5)$$

However, the exchange of N_2O between atmosphere and water alters the microbial isotopic signatures of N_2O in the water samples ($\delta_{i,\,water}$). A Keeling plot, based on the conservation of mass, can be applied to obtain the microbial isotopic signatures of N_2O and avoid bias derived from atmosphere-water exchange [63–65]. It assumes that the measured isotopic signature is a mixture of background atmosphere values and the microbial additions. The concentrations and isotopic signatures of dissolved N_2O were plotted with the atmospheric ones ($\delta^{15}N^{Bulk} = 6.55 \pm 0.47$, $\delta^{18}O = 44.4 \pm 0.34$ and $\delta^{15}N^{SP} = 19.4 \pm 1.92$) [49]. The isotopic signatures of microbially produced N_2O are represented as the y-intercept value. In addition, it is worth noting that N_2O may undergo reduction processes, which can significantly alter their original isotopic signatures ($\delta_{i,\,original}$). During N_2O reduction, the ratio between the isotope effects for $\delta^{15}N^{SP}$ and $\delta^{18}O$ remained relatively stable. Thus, the $\delta^{15}N^{SP}/\delta^{18}O$ map could be used to quantify the degree of N_2O reduction and calculate the original isotope source signatures (Fig. S5) [66,67].

Bayesian isotope mixing model

N_2O microbial sources can be quantified by distributing *in situ* isotopic signatures to each microbial process [48–50], which was realized by the Stable Isotope Mixing Models in R (SIMMR) [68]. The Stable Isotope Mixing Models were formulated as Eqs. 6–9:

$$X_{ij} = \frac{\sum_{k=1}^{K} p_k q_{jk}(s_{jk} + c_{jk})}{\sum_{k=1}^{K} p_k q_{jk}} + \varepsilon_{ij} \quad (6)$$

$$s_{jk} \sim N(\mu_{jk}, \omega_{jk}^2) \quad (7)$$

$$c_{jk} \sim N(\lambda_{jk}, \tau_{jk}^2) \quad (8)$$

$$\varepsilon_{ij} \sim N(0, \sigma_j^2), \quad (9)$$

where X_{ij} = observed isotope value j of the mixture i (i.e. $\delta_{i,\,original}$); s_{jk} = source value k on isotope j, normally distributed with mean μ_{jk} and variance ω_{jk}^2 (i.e. corrected values of denitrification, NDN and nitrification in Table S3); c_{jk} = fractionation factors for isotope j on source k, normally distributed with mean λ_{jk} and variance τ_{jk}^2. As the original isotope source signatures of N_2O before reduction were input in this study, the isotope fractionation factors $c_{jk} = 0$; p_k = proportion of source k, estimated by the model; q_{jk} = concentration of isotope j in source k; ε_{ij} = residual error, describing additional inter-observation variance not described by the model, while σ_j^2 was estimated by the model.

Because $\delta^{15}N^{Bulk}$ and $\delta^{18}O$ are dependent on the substrates, the exchange of O between H_2O and precursors of N_2O also perturbs $\delta^{18}O$ of N_2O, therefore we adopted corrected isotopic values to avoid bias from precursor substances [66,69]. The Kjeldahl distillation procedure was employed to measure the stable isotope ratios of $\delta^{15}N\text{-}NH_4^+$ [70]. NO_3^- was transformed into N_2O for determination of the $\delta^{15}N\text{-}NO_3^-$ and $\delta^{18}O\text{-}NO_3^-$ isotopes using denitrifying bacteria (*Pseudomonas aureofaciens*; ACTT 13985, USA). The isotopic signatures for each microbial process and precursors are listed in Table S3.

Management strategies

The difference in the N_2O partial pressure ($\Delta N_2O = N_2O_{water} - N_2O_{equilibrium}$) for global rivers was used to indicate the N_2O emission capacity. The air-water N_2O equilibrium concentration ($N_2O_{equilibrium}$) can be calculated via Eq. 10 [71]:

$$N_2O_{equilibrium} = K_h \times p_A = K_h \times C_A RT, \quad (10)$$

where $N_2O_{equilibrium}$ is the air-water equilibrium concentration of N_2O (nmol/L) and C_A is the atmospheric N_2O concentration. In the absence of local water temperature data, the existing saturation data of N_2O ($S = N_2O_{water}/N_2O_{equilibrium} \times 100\%$) were employed to calculate the ΔN_2O, $\Delta N_2O = N_2O_{water} \times (S\text{-}100\%)/S$.

Two scenarios were established for managing riverine N_2O emissions. Under Scenario 1, the reduction proportion for restoring hotspots to their baselines was calculated via Eq. 11:

$$\sum(\Delta N_2O_{i,hotspots} - \Delta N_2O_{A/U\,baseline})/\sum \Delta N_2O_i, \quad (11)$$

where $\Delta N_2O_{i,\,hotspots}$ is the ΔN_2O concentration at each hotspot; $\Delta N_2O_{A/U\,baseline}$ is the median ΔN_2O concentration in agricultural (23.9 nM) and urban (21.7 nM) rivers; and ΔN_2O_i is the ΔN_2O concentration at each sampling point in agricultural and urban rivers.

Under Scenario 2, a nitrate-based ΔN_2O reduction model was established, and restoration was performed from the highest unit benefits (slope, $\Delta N\text{-}N_2O/N\text{-}NO_3^-$). The $EF_{Control}$, median concentration, unit benefits and reduction proportion

were calculated for the hotspots and baseline points at 10% intervals (Table S4). For each group of sample points (e.g. 10%–20%), $EF_{Control}$ is the lowest slope ($\Delta N\text{-}N_2O/N\text{-}NO_3^-$) at the final order. Moreover, the unit benefit is the average $\Delta N\text{-}N_2O/N\text{-}NO_3^-$ value in this group. The reduction proportion for restoring the agricultural/urban hotspots and baselines to natural baselines was calculated via Eqs. 12 and 13, respectively:

$$\sum(\Delta N_2O_{i,hotspots} - \Delta N_2O_{Natural\ baseline})/\sum \Delta N_2O_i \quad (12)$$

$$\sum(\Delta N_2O_{i,10\%} - \Delta N_2O_{Natural\ baseline})/\sum \Delta N_2O_i, \quad (13)$$

where $\Delta N_2O_{i,hotspots}$ is the ΔN_2O concentration at each hotspot; $\Delta N_2O_{i,10\%}$ is the ΔN_2O concentration at the sampling points in agricultural and urban rivers at 10% intervals; $\Delta N_2O_{Natural\ baseline}$ is the median ΔN_2O concentration in natural rivers (0.02 nM); and ΔN_2O_i is the ΔN_2O concentration at each sampling point in agricultural and urban rivers.

DATA AVAILABILITY

All data used in this study are compiled into Supplementary data. Correspondence and requests for materials should be addressed to Guodong Ji (jiguodong@pku.edu.cn).

SUPPLEMENTARY DATA

Supplementary data are available at *NSR* online.

FUNDING

This work was supported by the Key Projects of the Joint Fund of the National Natural Science Foundation of China (U22A20557), the Autonomous Region Collaborative Innovation Center for Integrated Management of Water Resources and Water Environment in the Inner Mongolia Reaches of the Yellow River, and the National Natural Science Foundation of China (52379084).

AUTHOR CONTRIBUTIONS

Conceptualization was carried out by S.W. and G.D.J. Investigation and visualization were carried out by S.W. The original draft was written by S.W. Review and editing of the draft were carried out by W.Z., S.J.L., T.L. and G.D.J. Supervision was the responsibility of G.D.J.

Conflict of interest statement. None declared.

REFERENCES

1. Tian H, Xu R, Canadell JG *et al.* A comprehensive quantification of global nitrous oxide sources and sinks. *Nature* 2020; **586**: 248–56.
2. Yao Y, Tian H, Shi H *et al.* Increased global nitrous oxide emissions from streams and rivers in the Anthropocene. *Nat Clim Change* 2020; **10**: 138–42.
3. Wang G, Xia X, Liu S *et al.* Distinctive patterns and controls of nitrous oxide concentrations and fluxes from urban inland waters. *Environ Sci Technol* 2021; **55**: 8422–31.
4. Hu M, Chen D, Dahlgren RA. Modeling nitrous oxide emission from rivers: a global assessment. *Glob Change Biol* 2016; **22**: 3566–82.
5. IPCC. *2019 Refinement to the 2006 IPCC Guidelines for National Greenhouse Gas Inventories—IPCC*. 2019.
6. Song K, Senbati Y, Li L *et al.* Distinctive microbial processes and controlling factors related to indirect N_2O emission from agricultural and urban rivers in Taihu Watershed. *Environ Sci Technol* 2022; **56**: 4642–54.
7. Dong Y, Liu J, Cheng X *et al.* Wastewater-influenced estuaries are characterized by disproportionately high nitrous oxide emissions but overestimated IPCC emission factor. *Commun Earth Environ* 2023; **4**: 395.
8. Hu M, Li B, Wu K *et al.* Modeling riverine N_2O sources, fates, and emission factors in a typical river network of Eastern China. *Environ Sci Technol* 2021; **55**: 13356–65.
9. Soued C, del Giorgio PA, Maranger R. Nitrous oxide sinks and emissions in boreal aquatic networks in Québec. *Nat Geosci* 2016; **9**: 116–20.
10. Thompson RL, Lassaletta L, Patra PK *et al.* Acceleration of global N_2O emissions seen from two decades of atmospheric inversion. *Nat Clim Change* 2019; **9**: 993–8.
11. Maavara T, Lauerwald R, Laruelle GG *et al.* Nitrous oxide emissions from inland waters: are IPCC estimates too high? *Glob Change Biol* 2019; **25**: 473–88.
12. Zhi W, Klingler C, Liu J *et al.* Widespread deoxygenation in warming rivers. *Nat Clim Change* 2023; **13**: 1105–13.
13. Rosamond MS, Thuss SJ, Schiff SL. Dependence of riverine nitrous oxide emissions on dissolved oxygen levels. *Nat Geosci* 2012; **5**: 715–8.
14. Xu W, Wang G, Liu S *et al.* Globally elevated greenhouse gas emissions from polluted urban rivers. *Nat Sustain* 2024; **7**: 938–48.
15. Wang J, Vilmin L, Mogollón JM *et al.* Inland waters increasingly produce and emit nitrous oxide. *Environ Sci Technol* 2023; **57**: 13506–19.
16. Hu H-W, Chen D, He J-Z. Microbial regulation of terrestrial nitrous oxide formation: understanding the biological pathways for prediction of emission rates. *FEMS Microbiol Rev* 2015; **39**: 729–49.
17. Beaulieu JJ, Tank JL, Hamilton SK *et al.* Nitrous oxide emission from denitrification in stream and river networks. *Proc Natl Acad Sci USA* 2011; **108**: 214–9.

18. Sutka RL, Ostrom NE, Ostrom PH *et al.* Stable nitrogen isotope dynamics of dissolved nitrate in a transect from the north Pacific subtropical gyre to the eastern tropical north Pacific. *Geochim Cosmochim Acta* 2004; **68**: 517–27.
19. Chen X, Zhang S, Liu J *et al.* Tracing microbial production and consumption sources of N_2O in rivers on the Qinghai-Tibet plateau via isotopocule and functional microbe analyses. *Environ Sci Technol* 2023; **57**: 7196–205.
20. Liang X, Wang B, Gao D *et al.* Nitrification regulates the spatiotemporal variability of N_2O emissions in a eutrophic lake. *Environ Sci Technol* 2022; **56**: 17430–42.
21. Wang S, Lan B, Yu L *et al.* Ammonium-derived nitrous oxide is a global source in streams. *Nat Commun* 2024; **15**: 4085.
22. Li Y, Tian H, Yao Y *et al.* Increased nitrous oxide emissions from global lakes and reservoirs since the pre-industrial era. *Nat Commun* 2024; **15**: 942.
23. Wang J, Wang G, Zhang S *et al.* Indirect nitrous oxide emission factors of fluvial networks can be predicted by dissolved organic carbon and nitrate from local to global scales. *Glob Change Biol* 2022; **28**: 7270–85.
24. Borges AV, Darchambeau F, Teodoru CR *et al.* Globally significant greenhouse-gas emissions from African inland waters. *Nat Geosci* 2015;**8**: 637–42.
25. Upstill-Goddard RC, Salter ME, Mann PJ *et al.* The riverine source of CH_4 and N_2O from the Republic of Congo, western Congo Basin. *Biogeosciences* 2017; **14**: 2267–81.
26. Zhang L, Zhang S, Xia X *et al.* Unexpectedly minor nitrous oxide emissions from fluvial networks draining permafrost catchments of the East Qinghai-Tibet Plateau. *Nat Commun* 2022; **13**: 950.
27. Wang G, Wang J, Xia X *et al.* Nitrogen removal rates in a frigid high-altitude river estimated by measuring dissolved N_2 and N_2O. *Sci Total Environ* 2018; **645**: 318–28.
28. Galantini L, Lapierre J-F, Maranger R. How are greenhouse gases coupled across seasons in a large temperate river with differential land use? *Ecosystems* 2021; **24**: 2007–27.
29. Aho KS, Maavara T, Cawley KM *et al.* Inland waters can act as nitrous oxide sinks: observation and modeling reveal that nitrous oxide undersaturation may partially offset emissions. *Geophys Res Lett* 2023; **50**: e2023GL104987.
30. Begum MS, Bogard MJ, Butman DE *et al.* Localized pollution impacts on greenhouse gas dynamics in three anthropogenically modified Asian River systems. *J Geophys Res Biogeosci* 2021; **126**: e2020JG006124.
31. Chiriboga G and Borges AV. Andean headwater and piedmont streams are hot spots of carbon dioxide and methane emissions in the Amazon basin. *Commun Earth Environ* 2023; **4**: 76.
32. Borges AV, Darchambeau F, Lambert T *et al.* Variations in dissolved greenhouse gases (CO_2, CH_4, N_2O) in the Congo River network overwhelmingly driven by fluvial-wetland connectivity. *Biogeosciences* 2019; **16**: 3801–34.
33. Wang J, Wu W, Zhou X *et al.* Nitrous oxide (N_2O) emissions from the high dam reservoir in longitudinal range-gorge regions on the Lancang-Mekong River, southwest China. *J Environ Manage* 2021; **295**: 113027.
34. Li X, Sardans J, Qi M *et al.* Nitrous oxide concentration and flux in Min River Basin of southeast China: effects of land use, stream order and water variables. *J Hydrol* 2022; **614**: 128507.
35. Cooper RJ, Wexler SK, Adams CA *et al.* Hydrogeological controls on regional-scale indirect nitrous oxide emission factors for rivers. *Environ Sci Technol* 2017; **51**: 10440–8.
36. Webb JR, Clough TJ, Quayle WC. A review of indirect N_2O emission factors from artificial agricultural waters. *Environ Res Lett* 2021; **16**: 043005.
37. Yang L and Lei K. Effects of land use on the concentration and emission of nitrous oxide in nitrogen-enriched rivers. *Environ Pollut* 2018; **238**: 379–88.
38. Xiao Q, Hu Z, Fu C *et al.* Surface nitrous oxide concentrations and fluxes from water bodies of the agricultural watershed in Eastern China. *Environ Pollut* 2019; **251**: 185–92.
39. Grossel A, Bourennane H, Ayzac A *et al.* Indirect emissions of nitrous oxide in a cropland watershed with contrasting hydrology in central France. *Sci Total Environ* 2021; **766**: 142664.
40. Yu Z, Deng H, Wang D *et al.* Nitrous oxide emissions in the Shanghai river network: implications for the effects of urban sewage and IPCC methodology. *Glob Change Biol* 2013; **19**: 2999–3010.
41. Audet J, Bastviken D, Bundschuh M *et al.* Forest streams are important sources for nitrous oxide emissions. *Glob Change Biol* 2020; **26**: 629–41.
42. Thuan NC, Koba K, Yano M *et al.* N_2O production by denitrification in an urban river: evidence from isotopes, functional genes, and dissolved organic matter. *Limnology* 2018; **19**: 115–26.
43. Mishima I, Masuda S, Kakimoto T *et al.* Assessment of nitrous oxide production in eutrophicated rivers with inflow of treated wastewater based on investigation and statistical analysis. *Environ Monit Assess* 2021; **193**: 93.
44. Zhou Y, Toyoda R, Suenaga T *et al.* Low nitrous oxide concentration and spatial microbial community transition across an urban river affected by treated sewage. *Water Res* 2022; **216**: 118276.
45. Liu X-L, Bai L, Wang Z-L *et al.* Nitrous oxide emissions from river network with variable nitrogen loading in Tianjin, China. *J Geochem Explor* 2015; **157**: 153–61.
46. Chun Y, Kim D, Hattori S *et al.* Temperature control on wastewater and downstream nitrous oxide emissions in an urbanized river system. *Water Res* 2020; **187**: 116417.
47. Tian L, Cai Y, Akiyama H. A review of indirect N_2O emission factors from agricultural nitrogen leaching and runoff to update of the default IPCC values. *Environ Pollut* 2019; **245**: 300–6.
48. Yoshikawa C, Abe H, Aita MN *et al.* Insight into nitrous oxide production processes in the western North Pacific based on a marine ecosystem isotopomer model. *J Oceanogr* 2016; **72**: 491–508.
49. Snider DM, Venkiteswaran JJ, Schiff SL *et al.* From the ground up: global nitrous oxide sources are constrained by stable isotope values. *PLoS One* 2015; **10**: e0118954.
50. Yu L, Harris E, Lewicka-Szczebak D *et al.* What can we learn from N_2O isotope data?—Analytics, processes and modelling. *Rapid Commun Mass Spectrom* 2020; **34**: e8858.
51. Cline JD and Kaplan IR. Isotopic fractionation of dissolved nitrate during denitrification in the eastern tropical north pacific ocean. *Mar Chem* 1975;**3**: 271–99.
52. Moss B. Water pollution by agriculture. *Philos Trans R Soc B Biol Sci* 2007; **363**: 659–66.
53. Steffen W, Richardson K, Rockström J *et al.* Planetary boundaries: guiding human development on a changing planet. *Science* 2015; **347**: 1259855.
54. Zhang X, Davidson EA, Mauzerall DL *et al.* Managing nitrogen for sustainable development. *Nature* 2015; **528**: 51–9.
55. United Nations. Progress on Wastewater Treatment (SDG target 6.3). https://www.sdg6data.org/en/indicator/6.3.1 (6 January 2025, date last accessed).
56. Wu Y, Xi X, Tang X *et al.* Policy distortions, farm size, and the overuse of agricultural chemicals in China. *Proc Natl Acad Sci USA* 2018; **115**: 7010–5.
57. Deng O, Wang S, Ran J *et al.* Managing urban development could halve nitrogen pollution in China. *Nat Commun* 2024; **15**: 401.
58. Ricci GF, D'Ambrosio E, De Girolamo AM *et al.* Efficiency and feasibility of best management practices to reduce nutrient loads in an agricultural river basin. *Agric Water Manag* 2022; **259**: 107241.

59. Wang S, Li S, Ji M *et al.* Long-neglected contribution of nitrification to N_2O emissions in the Yellow River. *Environ Pollut* 2024; **351**: 124099.
60. Sander R. Compilation of Henry's law constants (version 4.0) for water as solvent. *Atmospheric Chem Phys* 2015; **15**: 4399–981.
61. Li X, Yu Y, Fan H *et al.* Intense denitrification and sewage effluent result in enriched ^{15}N in N_2O from urban polluted rivers. *J Hydrol* 2022; **608**: 127631.
62. Tischer J, Zopfi J, Frey C *et al.* Isotopic signatures of biotic and abiotic N_2O production and consumption in the water column of meromictic, ferruginous Lake La Cruz (Spain). *Limnol Oceanogr* 2022; **67**: 1760–75.
63. Li Q, Wang F, Yu Q *et al.* Dominance of nitrous oxide production by nitrification and denitrification in the shallow Chaohu Lake, Eastern China: insight from isotopic characteristics of dissolved nitrous oxide. *Environ Pollut* 2019; **255**: 113212.
64. Pataki DE, Ehleringer JR, Flanagan LB *et al.* The application and interpretation of Keeling plots in terrestrial carbon cycle research. *Glob Biogeochem Cycles* 2003; **17**: 1022.
65. Yamagishi H, Westley MB, Popp BN *et al.* Role of nitrification and denitrification on the nitrous oxide cycle in the eastern tropical North Pacific and Gulf of California. *J Geophys Res Biogeosci* 2007; **112**: G02015.
66. Lewicka-Szczebak D, Lewicki MP, Well R. N_2O isotope approaches for source partitioning of N_2O production and estimation of N_2O reduction—validation with the ^{15}N gas-flux method in laboratory and field studies. *Biogeosciences* 2020; **17**: 5513–37.
67. Wu D, Well R, Cárdenas LM *et al.* Quantifying N_2O reduction to N_2 during denitrification in soils via isotopic mapping approach: model evaluation and uncertainty analysis. *Environ Res* 2019; **179**: 108806.
68. Parnell AC, Inger R, Bearhop S *et al.* Source partitioning using stable isotopes: coping with too much variation. *PLoS One* 2010; **5**: e9672.
69. Lewicki MP, Lewicka-Szczebak D, Skrzypek G. FRAME—Monte Carlo model for evaluation of the stable isotope mixing and fractionation. *PLoS One* 2022; **17**: e0277204.
70. Ryu H-D, Kim S-J, Baek U *et al.* Identifying nitrogen sources in intensive livestock farming watershed with swine excreta treatment facility using dual ammonium ($\delta^{15}NNH_4$) and nitrate ($\delta^{15}NNO_3$) nitrogen isotope ratios axes. *Sci Total Environ* 2021; **779**: 146480.
71. Crusius J and Wanninkhof R. Gas transfer velocities measured at low wind speed over a lake. *Limnol Oceanogr* 2003; **48**: 1010–7.

Sustainable management of riverine N2O emission baselines

Wang, Shuo

2025-02-01

Wang S, Zhi W, Li S, et al., (2025) Sustainable management of riverine N2O emission baselines. National Science Review, Volume 12, Issue 2, February 2025, Article number nwae458 https://doi.org/10.1093/nsr/nwae458